Chapter II
Literature Review

II.1 Review of Earthquake Site Characterization

II.1.1 Attenuation Function

Since the probabilistic seismic hazard are not peformed in this research, target spectra (it is called by uniform hazard spectra in some references) is derived by deteriministic seismic hazard criteria using appropriate attenuation function for site interest. This earthquake scenarios are designed to be different from subduction and strike slip mechanism. The subduction will be represented both far and near source earthquake, while the strike slip is designed just to demonstrate the near source earthquake. Some magnitudes and closest distances are varied to obtain the interest of peak base acceleration. Common typical form of attenuation function is written in the form of

$$\ln Y = C_1 + C_2 + C_3 M^{C4} + C_5 \ln[R + C_6 \exp(C_7 M)] + C_8 R + \varepsilon \qquad \textbf{(2.1)}$$

where:

Y = ground motion amplitude

M = magnitude

R = distance

e = random component of logarithm of groun motion when magnitude and location are known

C_1,...C_8 are represented the characteristic coefficient which is referred to the researcher.

First, two attenuation function is chosen to represent each earthquake mechanism. For subduction, Atkinson-Boore (2003) and Youngs (1997) are apllied while Idriss (2004) and Sadigh (1997) function for the strike slip mechanism.

Following equation that form those attenuation functions which is used in this study are described as follows:

- ***Youngs, 1997*** : Subduction mechanism

$$\ln(y) = 0.2418 + 1.414M + C_1 + C_2(10-M)^3 + C_3 \cdot \ln(r_{rup} + 1.7818 \cdot e^{0.554M}) + 0.00607 \cdot H + 0.3846 \cdot Z_t \quad \textbf{(2.2a)}$$

$$\sigma_{\ln Y} = C_4 - C_5 \cdot M$$

where:

y = spectral acceleration in g

M = moment magnitude

H = depth in km

R or r_{rupt} = closest distance to rupture in km

- ***Atkinson-Boore*, *2003*** : Subduction mechanism

$$\ln Y = f_n(M) + C_3 h + C_4 R - g \log R + C_5 sl\ S_C + C_6 sl\ S_D + C_7 sl\ S_E \quad \textbf{(2.2b)}$$

where:

$f_n(M)$ = $C_1 + C_2 M$

g = $10^{(1.2-0.18M)}$ for interface events

= $10^{(0.301-0.01M)}$ for intraslab events

S_C, S_D and S_E = NEHRP site class

- ***Sadigh et al.*, *1997*** : Strike slip mechanism

$$\ln Y = C_1 + C_2\ M + C_3(8.5\ M)^{2.5} + C_4 \ln[r_{rup} + \exp(C_5 + C_6 M)] + C_7 \ln(r_{rup} + 2) \quad \textbf{(2.3a)}$$

where:

M = moment magnitude

R = closest distance to rupture surface

- ***Idriss, 204*** : Strike slip mechanism

$$\ln Y = [\alpha_0 + \exp(\alpha_1 + \alpha_2 M)] + [\beta_0 - \exp(\beta_1 + \beta_2 M)]\ln(R+20) + 0.2F + \varepsilon \quad \textbf{(2.3b)}$$

where:

M = magnitude, M_L for $M < 6$ and M_s for $M > 6$

F = fault style (0 for strike slip, 1 for reverse, 0.5 for oblique)

II.1.2 Strong Ground Motion

Seismic design criteria are most frequently represented using the response spectrum. If the design is based on a scenario earthquake, then earthquake magnitude and distance that the response spectrum represents are clearly defined, and it is a straightforward to select or generate ground motion time histories that represent this magnitude and distance. It is more common for the design spectrum to be based on a probabilistic seismic hazard analysis, representing ground motion level having a specified annual probability of excedance. The probability response spectrum then represents not a single earthquake magnitude and distance, but the aggregated contribution of a range of earthquake magnitude occurring at various rates on each of several distance faults or seismic source zones located at various distance from the site.

It also includes the effects of random variability in the ground motions for a given magnitude and distance. However, in order to provide ground motion time histories that are representative of the response spectrum, we must choose one or more discrete combinations of magnitude, distance, and epsilon, ε (number of standard deviation) to represent the probabilistic ground motion. The magnitude, distance and epsilon values are estimated through de-aggregation of the probabilistic seismic hazard using the procedure described by McGuire (1995).

When strong ground motion recordings are not available, simulated earthquake motions are used for a particular earthquake engineering application. Simulated earthquake motions represent synthetic data that can be used to supplement or supplant recorded motions. Two applications of simulations have been common in

engineering design practice: (1) to provide design ground motions for structural or geotechnical response analyses for a particular project site and (2) to provide synthetic for region (geographic area, magnitudes, and distances) of sparse data in developing design ground motion.

Artificial earthquake motion is defined by synthetic earthquake motion. For dynamic analysis due to earthquake excitation load, time-domain earthquake acceleration is required to determine the characterized earthquake design. There are three alternatives to perform earthquake design as the following:

1. Using earthquake data recording at certain site that have the typical geologic and tectonic condition to the observed site
2. Using scaled earthquake data recording at certain site which is associated to the observed site condition
3. Create an artificial earthquake motion that based on spectral design or spectral density function of the observed site.

In this research, the third alternatives are performed to create the earthquake motion. As described in the preceding section, the historical earthquake data are applied by conducting spectral matching technique. This spectral matching technique will obtain the characteristic ground motion appropriate to the expected target spectra design which is determined by atenuation function for both subduction and strike slip earthquake scenario. Moreover, these input motions are then assumed correspond with seismic return period 500 years.

II.1.3 Earthquake Characteristic

The significant earthquake characteristics in the earthquake engineering research are as follows:

1. Maximum spectral parameters (i.e. acceleration, velocity and displacement acceleration)
2. Earthquake duration
3. Frequency content

Each of the above parameter is influenced the response of the structure during earthquake. Maximum spectral acceleration is much influenced the amplitude vibration, whereas the earthquake duration will be influenced the magnitude strength vibration. The relatively small earthquake magnitude with long enough duration is more damage than the large earthquake magnitude but has shorter duration. Furthermore, the frequency content and spectral envelope is related to frequency and period of structure. When the frequency of soil is equal to frequency of the structure, the soil earthquake vibration will be amplified on the structure. This phenomenon is known by resonance effect.

II.2 Ground Response

Geotechnical earthquake engineering usually encounter the ground response analysis in order to provide the behavior of the seismic load travel the soil layer. Ground response analyses are accounted to develop the solution for surface design rensponse spectra, to evaluate dynamic stress and strains for evaluation of liquefaction hazards, and to determine the dynamic earthquake-induceed forces that can lead to instability of earth retaining structures or lateral deformation of pile foundation.

Each of the above problem must fistly be considered the wave propagation from earthquake source to reach the site interest. In this section, ground response analysis will start on the dynamic properties of soil, local site class and an introduction to synthetic input motion and soil-structure method.

II.2.1 Dynamic Properties of Soil

The relationship of soil stress-strain due to insitu stress, joint, discontinuity, load history, temperature and pore water pressure are non-trivial and non-linear solution. The non-linearity of soil is occurred due to deformation of soil, then the stiffness of soil will be changed as well after loading was mobilized. This non-linearity behavior of soil was well-known and applied in the soil model comprehensively especially for soil-deformation analysis under static load.

Otherwise, linear approach have to be modified to give the optimum soil responses estimation in the practical cases subjected to dynamic loading. The actual behavior of non-linear stress-strain relationship of soil during cyclic or earthquake excitation load can be investigated by linear equivalent of soil properties. Equivalent shear modulus, G is obtained from secant shear modulus and equivalent damping ratio, ξ which have the same loss of energy cycle in the actual hysteresis loop.

Because linear approach needs the constant value of G and ξ for each soil layer, the parameters must be consistent to the stress level for each soil layer too. This is a matter of problem to be solved carefully. To perform the above analysis, laboratory test is performed to investigate the character of equivalent strain level to the shear strain of a actual earthquake motion. The result shows that empirical effective shear strain will be varied in range of 50%-70% of maximum shear strain from laboratory test. However, shear strain is often stated in the 65% of maximum shear strain because of the above value is not too sensitive.

To estimate the properties of soil for the linear approach, the consistent correlation are well defined in earthquake codes such as Uniform Building Code (UBC), National Earthquake Hazards Reduction Program (NEHRP) or Standar Nasional Indonesia (SNI). Those properties which are classified by UBC are presented in the following section. It can be seen that the SNI classification is also consistent with UBC site class. The propoerties of linear behavior of soil is usually defined in term of average shear wave veocity, v_s and equivalent (maximum) shear modulus, G, which is stated in the formula below.

$$G = \rho * v_s^2 \qquad \textbf{(2.4)}$$

$$\rho = \frac{\gamma}{g} \qquad \textbf{(2.5)}$$

where,

v_s = shear wave velocity

γ = total unit weight

g = gravity acceleration (9.81 m/sec^2)

To elucidate the one-dimensional wave propagation analysis, other parameters can be derived from the above formula and, as the following.

$$v_p = \sqrt{\frac{E_{oed}}{\rho}} \quad \textbf{(2.6)}$$

$$E_{oed} = \frac{(1-\upsilon)E}{(1+\upsilon)(1-2\upsilon)} \quad \textbf{(2.7)}$$

$$E = G\,(1 + 2\nu) \quad \textbf{(2.8)}$$

where,

v_p = pressure (compression) wave velocity

E = Young's modulus

E_{oed} = one-dimensional stiffness of soil

II.2.2 Local Site Class

Uniform Building Code (UBC), 1997 classified local site class into 6 (six) classes using shear wave, V_s parameter, SPT value, N-SPT or undrained shear strength of soil, s_u up to 30m depth of soil layer as shown in the **Table 2.1** below. This classification is consistent to the other local site classification such as, Standar Nasional Indonesia (SNI) 2002, National Earthquake Hazard Reduction Program (NEHRP) 1997, Borcherdt (1994), Boore et, all (1993) and many researchers.

II.2.3 Synthetic Earthquake Input Motion

Synthetic input motion in this research is obtained by spectral mathing method that proposed by Norm Abarhamson (2003). Based on the proposed method, the motion will be scored to the target spectra by the *rms* acceleration, duration and Arias intesity. A rms acceleration is defined by parameter that include the effects of the amplitude and frequency content of a strong motion record, written in the equation below.

Table 2.1 Local Site Class based on UBC 1997

Site Class	Description	$\bar{V}_s$	$\bar{N}$ - SPT	$\bar{s}_u$
		m/sec	blows/30cm	kPa
S_A	Hard Rock	Vs > 1500	-	-
S_B	Rock	760 < Vs ≤ 1500	-	-
S_C	Soft Rock or Very Dense Soil	360 < Vs ≤ 760	N > 50	s_u > 100
S_D	Medium of Stiff Soil	180 < Vs ≤ 360	15 < N ≤ 50	50 < s_u ≤ 100
S_E	Soft Soil	Vs ≤ 180	N ≤ 15	s_u ≤ 50
S_F	Special Soil	Liquefable or soft to medium clay greater than 30m-depth		

$$a_{rms} = \sqrt{\frac{1}{T_d}\int_0^{T_d}[a(t)]^2 dt} = \sqrt{\lambda_o} \qquad \textbf{(2.9)}$$

where T_d is the duration of strong motion and λ_o is the average intensity (or mean square acceleration)

whereas the Arias Intensity is the parameter closely to related to the above rms acceleration, formulated by

$$Ia = \frac{\pi}{2g}\int_0^{\infty}[a(t)]^2 dt \qquad \textbf{(2.10)}$$

Since its obtained by integration over the entire duartion rather than over the duration of strong motion, its value is independent of the method used to define the duration of strong motion

II.3 Review of Seismic Soil-Pile-Superstructure Interaction (SSPSI) subjected to some Great Earthquakes

Recently, many researchers have intensively studied the behavior of seismic soil-pile-siperstructure interaction (it will be abbreviated to be SSI in this research consistently) especially for the structure sited on the soft ground. The development of the study is then enriched by the fact of structure response during great earthquake over the decades. Herein, some of the great earthquakes are reviewed and how the soil-fondation-structure interact within is then investigated. For the sake of introductory review, the principal characteristics of seismic soil-pile-superstructure interaction (SSI) for an individual pile are illustrated schematically in **Figure 2.1**. The system components include the superstructure, the pile cap, the pile(s), the soil (here idealized into near field and far field domains), and the seismic energy source. **Figure 2.2** is then presented a sketch illustrating the key features and introducing the basic terminology in SSPSI analysis.

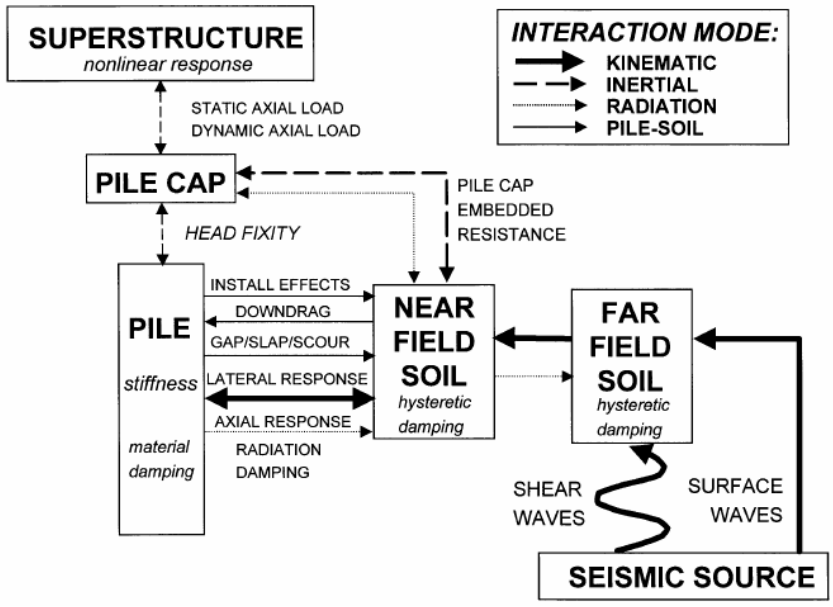

Figure 2.1 Schematic of modes of single-pile seismic response (after Meymand, 1998)

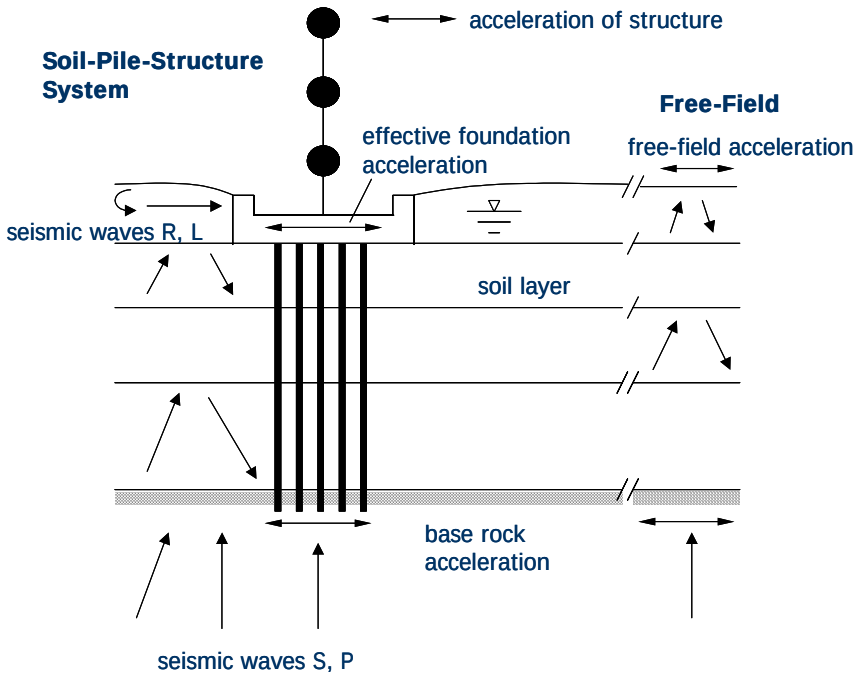

Figure 2.2 Schematic of soil-pile-structure interaction problem (after Gazetas, 1998)

II.3.1 The San Fernando Earthquake of February 9, 1971

The major collapsed concrete box girder spans of Golden State Freeway/Foothill Freeway Interchange bridges was found during this earthquake. Further, it was found that the epicenter of the magnitude 6.4 San Fernando Earthquake very close to the bridges that less than 10 miles. The soil condition at the interchange of single pier to the foundation is dense silty sand. The failure of the bridge pier was typially concentrated at the base of this columns, because the main reinforcing bars in to the pile was overstressed during excitation load. Failure of the bridge column is illustrated in the **Figure 2.3** below.

It will be then investigated that near source earthquake results the major strucutural damages sited on the dense or hard layer.

Figure 2.3 Failure at connection detail between drilled shaft and bridge column at the Golden State Freeway/Foothill Freeway Interchange during San Fernando Earthquake (after Penzien, 1971)

II.3.2 The Mexico City Earthquake of September 19, 1985

The Michoacan, Mexico City of September 19, 1985 was quite large, its great distance from Mexico City produced accelerations at the rock site only 0.03 to 0.04g. With the magnitude 8.1, this wave travelling reach the site on the three different subsurfaces condition, Foothill, Transition and Lake Zone. Strucutural damage due to this seismic excittion was highly selective, lare parts of the city experience no damage while other areas suffered pronounced damage. Foothill and Transition zone almost had no structural damage, while the greatest damage occured at the Lake Zone. The site profile and dramatic damage building tduring this seismic excitation as shown in **Figure 2.4**.

Rigorous study shows that the damage to buildings of less than five stories and modern building greater than 30-stories were slight. Most building in the five-to 20-storey range, however, either collapsed or were badly damaged. Using the crude rule of thumb that the fundamental period of N-storey building is

approximately N/10 sec, most of these damaged buildings had fundamental periods equal to or somewhat less than characteristic site period which is estimated two seconds. This long period motion came into resonance with many structures of intermediate height, resulting a damage pattern closely focused on these long period structures. More over, these intermediate height of structures were experiencing "double resonance" condition, first amplification of bedrock motion by the soil deposit and second, amplification of the soil motion by the structure. Combining with the structural design and deficiencies to cause locally devastating damage.

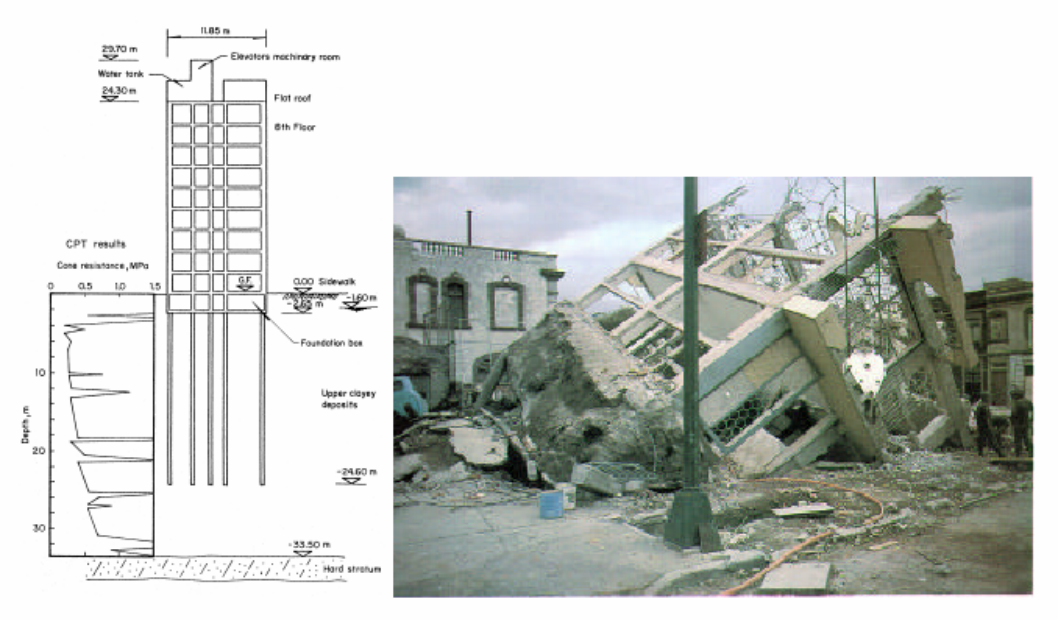

Figure 2.4 Ten story pile supported building founded on soft soils during the 1985 Mexico City Earthquake; Left: Elevation including geotechnical information, Right: Overturned Structure (after Mendoza and Auvinet, 1988)

II.3.3 The Loma Prieta Earthquake of October 19, 1989

During this earthquake, SSPSI play an imporant role to study how the damage was primarily a structural failure, however the fondation behavior greatly influences the collapsed structural mechanism. The magnitude 7.0 Loma Prieta earthquake, which is also called by San Fransisco Bay earthquake was occured beneath the basin that largely filled with alluvial deposits of clays and silty to sandy clays with some layers of sandy and gravelly soils. The fact shows that the earthquake caused extensive damage in certains areas, and relatively little damage in others, it will be then investigated that the local site effects were important to analyzed comprehensively.

Based on the above site condition, the structural failure was not contributed by the soil liquefaction as the upper foundations soil consisted of soft clays and organics, with some alluvial present. The punched lateral failure mechanism that indicating inadequate lateral support of soil resulted excessive lateral pile deflections, and flexural/shear failures at the pile to bent connections. Some documented photograps are presented as shown in **Figure 2.5** to **Figure 2.7**.

Figure 2.5 Highway 1 Crossing Struve Slough near Watsonville Collapsed during the 1989 Loma Prieta Earthquake, with Pile Punching through Deck (after Seed et al.,1990)

Figure 2.6 Formation of gap adjacent to one of the piles supporting collapsed Struve Slough Crossing during the 1989 Loma Prieta Earthquake (Seed et al.,1990)

Figure 2.7 Flexural shear failure of pile to bent connection of the Struve Slough Crossing during the 1989 Loma Prieta Earthquake (Seed et al.,1990)

II.3.4 The Hyogoken-Nanbu (Kobe) Earthquake of January, 1995

The University of Berkeley, California reported on its review after the 7.2 Kobe earthquake, it was the most destructive earthquake to strike Japan in over 60 years and devastated of all modes of infrastrucutures. The SSPSI was then analyzed the collpase of an elevated section of the pile supprted Hanshin Expressway as shown in **Figure 2.8**, one of the most dramatic structural failure during the Kobe earthquake. Due to the foundation flexibility, Gazetas and Mylonakis (1998) suggested that the foundation experience the period lengthening during earthquake and finally will increase strucutral forces as indicated by response spectra in **Figure 2.9**. Using the sub-structure method, Gazetas and Mylonakis was then re-analyzed the predominant period of the structure by comparing with soil-structure interaction and fixed-base system analysis.

Pile damage due to lateral spreading and superstructure inertial forces are presented in **Figure 2.10** to **Figure 2.11** to learn how SSPSI influence the behavior of the whole system.

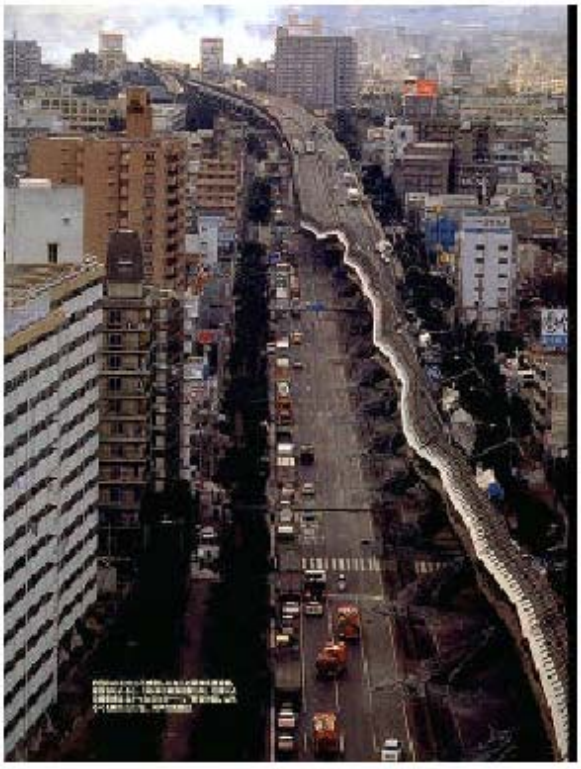

Figure 2.8 Collapsed Section of Hanshin Expressway

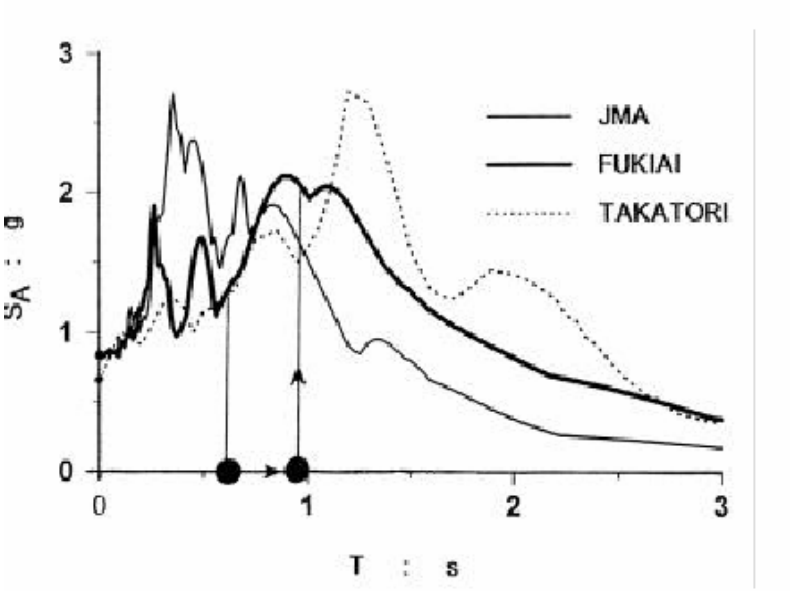

Figure 2.9 Response spectra recorded in vicinity of collapsed Hanshin Expressway illustrating effects of period lengthening due to foundation flexibility on increased structural forces (after Gazetas and Mylonakis, 1998)

Figure 2.10 Lateral spreading damage to pile during the 1995 Kobe Earthquake (after Tokimatsu et al., 1996)

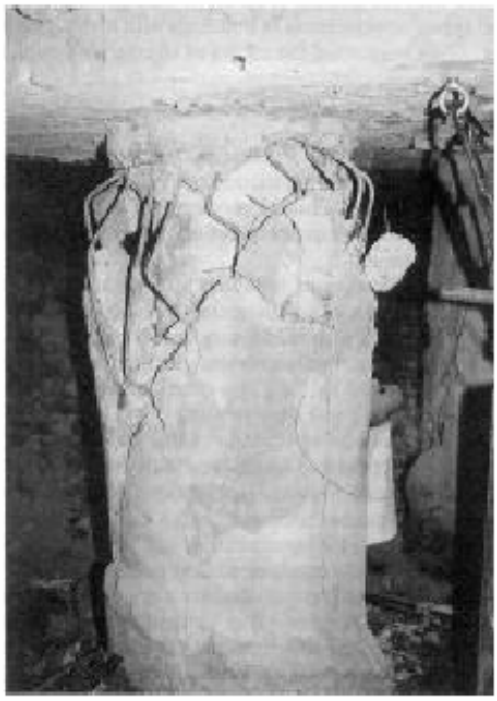

Figure 2.11 Pile damaged by superstructure inertial forces during the 1995 Kobe Earthquake (after Tokimatsu et al., 1996)

II.4 Review of Previous Work on Seismic Soil-Pile-Superstructure Interaction (SSI) Analysis

Particular modes of damage and failure of pile group foundation related to both kinematic and inertial interaction is illustrated in **Figure 2.12.** Loss of lateral soil support has been observed to occur due to liquefaction of cohesionless soils or strain softening of cohesive soils near the pile head. When combined with large structural inertial loads, excessive displacement sand bending strains concentrated near the pile head have developed and resulted in pile damage, frequently at the pile to cap connection.

Another common liquefaction hazard arises from the large loads that laterally spreading soil deposits exert on piles, which has frequently resulted in pile and structural damage. When soils along the length of the pile soften due to liquefaction or strain softening, piles have experienced a loss of bearing capacity,

and if combined with a rocking mode induced by superstructure inertial forces, the piles frequently undergo settlement, punching, or tensile pull-out failure.

Piles may also be subject to damaging bending strains at interfaces between soil layers of strong impedance contrast. This contrast may be provided by soft and stiff soil layers, or by soil layers that undergo liquefaction or strain softening under earthquake loading. Finally, battered (inclined) piles can form relatively stiff lateral resistance systems, and attract forces that the pile head and/or pile cap cannot sustain.

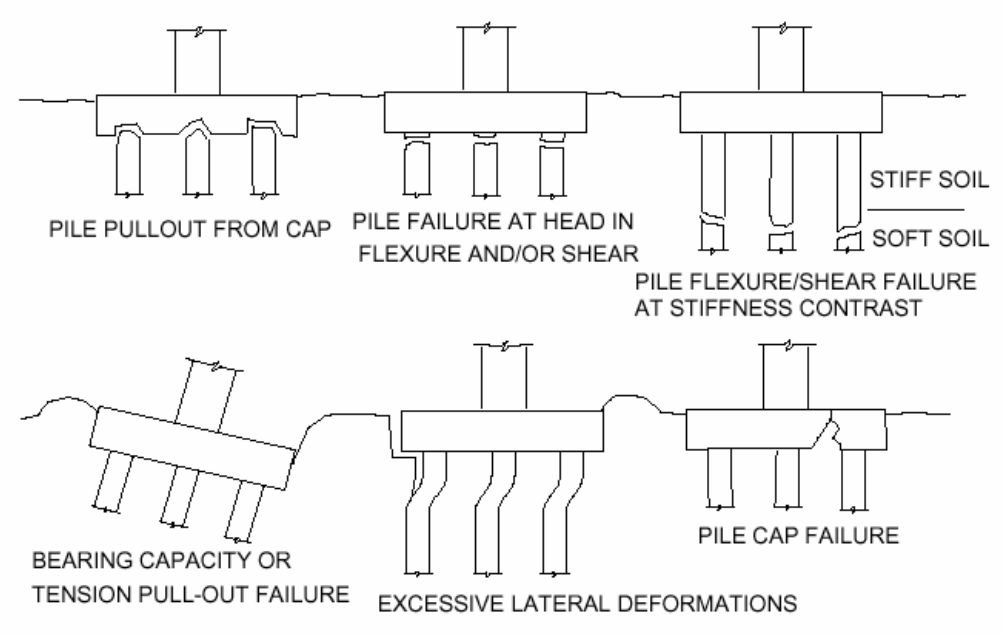

Figure 2.12 Potential failure modes for pile group foundation subjected to seismic load (after Meymand, 1998)

The development of analytical methods for SSI has principally been driven by the demands of two sectors, offshore oil production activities , and to a lesser extent, the nuclear power industry. For offshore applications, where cyclic wave loading applies lateral loads to pile-supported marine structures, a limited series of field and model tests has established the empirically-based and widely accepted “p-y” method of laterally loaded pile analysis.

The following sections will present a brief overview of four types of SSI analyses; these generally fall into the discrete and continuum classes model. For over recently 10-years, more complete reviews are available by Novak (1991), Gohl (1993), or Gazetas and Mylonakis (1998).

II.4.1 Beam-on-elastic foundation

Hetenyi (1946) originally presented beam-on-elastic foundation solutions (also known as the subgrade reaction method) in the form of the governing fourth order differential equation:

$$EI\frac{d^4y}{dx^4} = p \qquad \textbf{(2.11)}$$

where E and I are the pile modulus of elasticity and moment of inertia, y is the pile deflection, and p is the reaction of soil on the pile.

As is the case with the elastic continuum method, analytical solutions are not available for arbitrary distributions of soil or pile stiffness. This method has mainly been applied to static lateral pile loading problems, and is therefore used for the determination of pile head stiffness terms in SSI analyses. Matlock and Reese (1960) presented a generalized iterative solution method for rigid and flexible laterally loaded piles embedded in soils with two forms of varying modulus with depth. This method has mainly been applied to static lateral pile loading problems, and is therefore used for the determination of pile head stiffness terms in SSPSI analyses.

In classic companion papers, **Broms (1964a, b)** described a method for analyzing lateral pile response in cohesive and cohesionless soils. His method for computing ground surface deflections of rigid and flexible fixed and free head piles was based on a modulus of subgrade reaction using values suggested by Terzaghi (1955). For undrained loading, he designated that a constant subgrade modulus be used with a value of 9 Su for the ultimate lateral soil resistance. For drained loading cases, a subgrade modulus linearly increasing with depth was specified and a Rankine earth pressure-based method was used for computing an ultimate resistance assumed equal to 3KpDpσ'v.

Kulhawy and Chen (1995) applied Brom's concepts to drilled shafts, recognizing the components of resistance to lateral loading unique to drilled shafts, and noted the importance of conducting appropriate laboratory tests for laterally loaded pile and drilled shaft analysis.

II.4.2 Beam-on-Winkler foundation

By accepting Winkler's foundation assumption (1876) that each layer of soil responds independently to adjacent layers, a beam and discrete spring system may be adopted to model pile lateral loading. Although this assumption ignores the shear transfer between layers of soil, it has proven to be a popular and effective method for static and dynamic lateral pile response analyses. In this method, the soil-pile contact is discretized to a number of points where combinations of springs and dashpots represent the soil-pile stiffness and damping at each particular layer. These soil-pile springs may be linear elastic or nonlinear; p-y curves typically used to model nonlinear soil-pile stiffness have been empirically derived from field tests, and have the advantage of implicitly including pile installation effects on the surrounding soil, unlike other methods.

In advanced applications, capabilities for soil-pile gapping, cyclic degradation, and rate dependency are also provided. A singular disadvantage of a beam-on-Winkler-foundation model is the two-dimensional simplification of the soil-pile contact, which ignores the radial and three dimensional components of interaction. **Figure 2.13** sketches this Beam-on-dynamic-Winkler-Foundation (BDWF).

Matlock and his co-workers conducted static and cyclic field and laboratory tests of laterally loaded piles in soft clay. He described the p-y concept as the relationship that relates the soil resistance "p" arising from the non-uniform stress field surrounding the pile mobilized in response to a lateral soil displacement "y" as illustrated in **Figure 2.14**. For a single pile, a family of p-y curves can be described normally stiffer with depth as shown in **Figure 2.15** as the following.

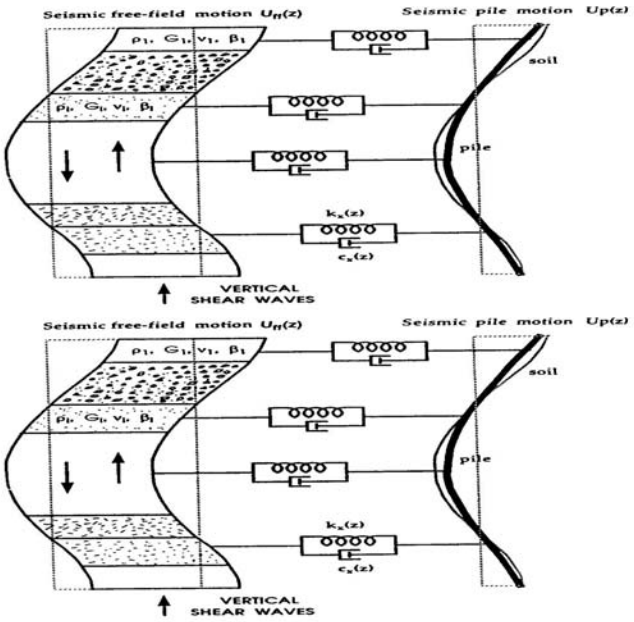

Figure 2.13 Beam-on-Dynamic-Winkler-Foundation (BDWF) model for soil-pile interaction analysis in multi-layered soil

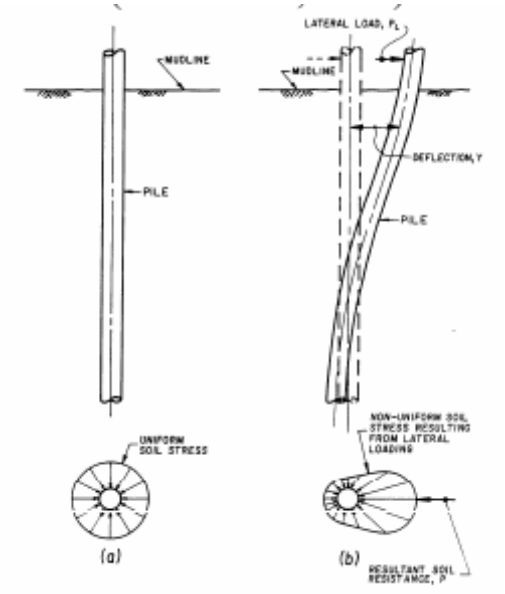

Figure 2.14 Definition of p-y concept with, a) pile at rest;

b) Lateral loaded pile mobilizing soil resistance (after Thompson, 1977)

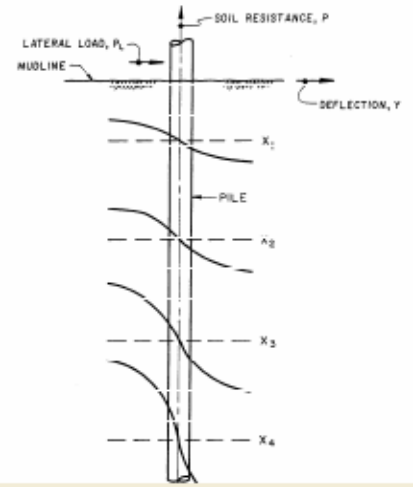

Figure 2.15 Typical family of p-y curves, progressively stiffer with depth (after Meyer and Reese, 1979)

Kagawa and Kraft (1980) developed a nonlinear dynamic Winkler model using the equivalent linear method, with input excitation applied as lateral ground displacements at the end of the near-field soil elements. The pile was modeled by a continuous beam with near field soil elements comprised of parallel springs and dashpots, and with superstructure elements that generated the inertial component of response. Soil spring stiffness values were determined from the hysteretic backbone curve and the radiation damping dashpot coefficient was computed as

$$c = 2\,\rho_s\,B\,(V_p + V_s) \qquad \textbf{(2.12)}$$

For dynamic loadings, "free-field" soil acceleration time histories are usually computed in a separate site response analysis, double integrated to displacement time histories, and then externally applied to the soil-pile springs. The multi-step uncoupled approach has the disadvantage of potentially introducing numerical errors in the integration step, and artificially separates the overall soil-pile system response. Recently, investigators have begun to develop fully-coupled analyses wherein both soil and soil-pile-superstructure response can be simultaneously evaluated **(Lok, 1999).**

II.4.3 Elastic continuum analysis

The elastic continuum analytical method is based on **Mindlin's (1936)** closed form solution for the application of point loads to a semi-infinite mass. The accuracy of these solutions is directly related to the evaluation of the Young's modulus and the other elastic parameters of the soil. This approach is limited in the sense that nonlinear soil-pile behavior is difficult to incorporate (the equivalent linear method is available), and it is more appropriately applied for small strain, steady state vibration problems. In addition, layered soil profiles cannot be accommodated, and only solutions for constant, linearly increasing, and parabolically increasing soil modulus with depth have been derived. True continuum models do have the advantage of intrinsically modeling the effects of radiation damping, whereas discrete models must artificially simulate this energy dissipation mode.

Poulos (1971a, b) published elastic continuum solutions for laterally loaded single piles and groups under static loading. Poulos and Davis (1980) presented a comprehensive set of analysis and design methods for pile foundations based on elastic continuum theory. Poulos (1982) described a procedure for degradation of soil-pile resistance under cyclic lateral loading and compared it to several case studies. In a different approach, Swane and Poulos (1984) proposed a subgrade reaction method that provided for progressive soil-pile gapping with bilinear elasto-plastic springs and friction slider blocks. In the 29th Rankine Lecture, Poulos (1989) presented a compendium of his work on axial pile loading.

Gazetas and Dobry (1984) derived a method for substructuring the SSPSI problem into kinematic and inertial components from a parametric finite element study based on the work of Blaney et al. (1976). For the inertial interaction component, they described the pile head dynamic stiffness by a complex valued impedance function of the form

$$K + i\,\omega\,C = p_o/y_d \qquad \textbf{(2.13)}$$

where K is the soil-pile stiffness, ω is the excitation frequency, C is the coefficient of equivalent viscous damping, po is the amplitude of the

forcing function, and yd is the complex amplitude of the horizontal motion.

Constant, linearly varying, and parabolically varying soil modulus with depth cases were studied for single piles subjected to vertically propagating shear waves. Kinematic interaction factors were graphically presented as functions of D, B, Ep, Es, ω and site frequency f; these curves are multiplied against free-field response spectra to yield design pile head response spectra. They also included a discussion of radiation damping models and proposed a simplified plane strain version as a function of B, rs, Vs, and ω as presented in **Figure 2.16**. This model for radiation damping emanating from a laterally oscillating pile consisted of zones of waves traveling at the soil shear wave velocity Vs, and at Lysmer's analog velocity V_{LA}, where:

$$V_{LA} = \frac{3.4V_s}{\pi(1-\upsilon)} \qquad \textbf{(2.14)}$$

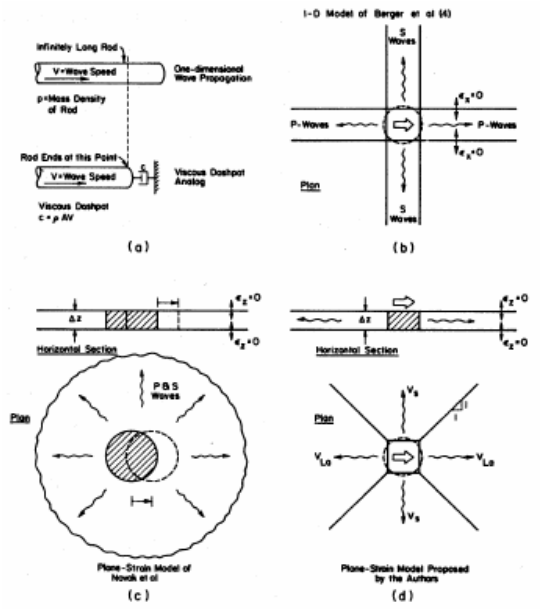

Figure 2.16 One- and two-dimensional radiation damping models (after Gazetas and Dobry, 1984)

II.4.4 Finite element method

The finite element method potentially provides the most powerful means for conducting SSPSI analyses, but is has not yet been fully realized as a practical tool. The advantages of a finite element approach include the capability of performing the SSPSI analysis of pile groups in a fully-coupled manner, without resorting to independent calculations of site or superstructure response, or application of pile group interaction factors. It is of course possible to model any arbitrary soil profile, and to study 3-D effects. Challenges to successful implementation of this technique lie in providing appropriate soil constitutive models that can model small to very large strain behavior, rate dependency, degradation of resistance, and still prove practical for use. Special features to account for pile installation effects and soil-pile gapping should also be implemented. However, finite element is most frequently used in practice at this time. The method is well suited for analyzing problems with analytical or semi-analytical formulation

Based on work by **Kausel et al. (1975)**, used a finite element formulation with a consistent boundary matrix to represent the free-field, subjected to both pile head and seismic base excitations, and derived dynamic pile stiffness coefficients as a function of dimensionless frequency. **Blaney et al. (1979)** have applied the viscous boundary to the dynamic analysis of a pile subjected either to lateral loading as its head or to base-rock-type of steady-state excitation. Thus, they obtained information pertaining to both inertial and kinematic pile-soil interaction.

Wu and Finn (1997a, b) presented a quasi-3-D finite element formulation with relaxed boundary conditions that permitted: a) dynamic nonlinear analysis of pile groups in the time-domain, and b) dynamic elastic analysis of pile groups in the frequency-domain. These methods showed good comparison to more rigorous techniques, but at reduced computational cost.

The most comprehensive analysis in soil-pile-superstructure interaction are performed by **Gazetas et al (1998)** in order to obtain structural period on the Hanshin Expressway structure during the 1985 Kobe earthquake. The analysis

was conducted by using the sub-structure methods as illustrated in **Figure 2.17**. The result is presented by comparison between including and excluding the SSI effects **(Figure 2.18).**

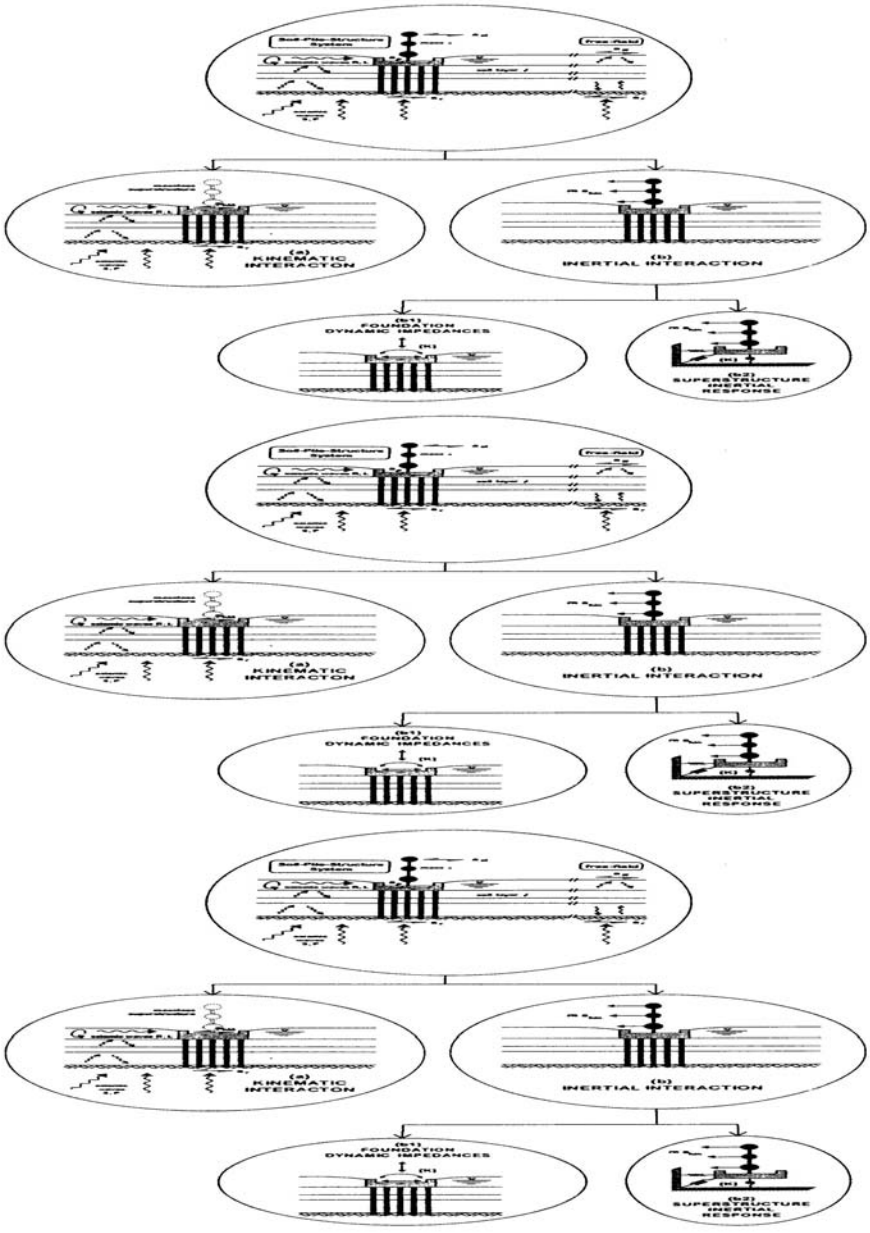

Figure 2.17 Decomposition of seismic soil-pile-structure response into kinematic and inertial interaction (after Gazetas et al, 1998)

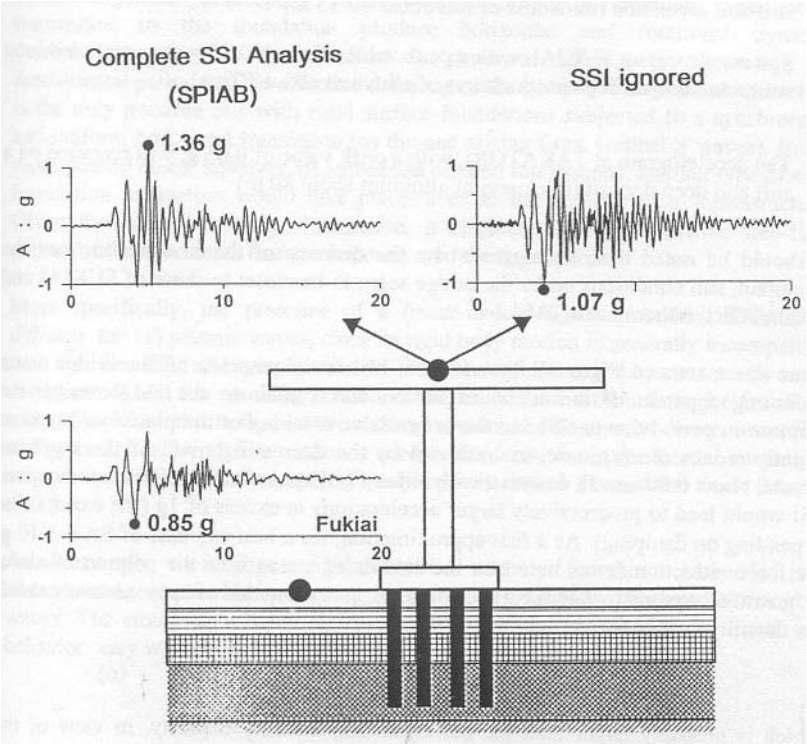

Figure 2.18 Effect of dynamic SSI on the acceleration response of the failed Route 3 Section of the Hanshin Expressway (after Gazetas et al, 1998)

II.5 Seismic Soil-Structure Interaction Analysis Using Finite Element Procedures

During the couple of decades it has been well-recognized that the soilon which a structure is construcuted may interact seismically with the structure during earthquakes, especially when the soil is relatively soft and the structure is stiff/rigid. This kind of seismic soil-structure interaction can sometimes modify significantly the stresses and deflections of the whole structural system from the values that could have been developed if the structure were constructed on rigid foundation. And two important characteristics that distinguish the seismic soil-structure system from other general dynamic structural systems are the unbounded nature and the non-linearity of the soil medium.

II.5.1 Developing History

Modeling and analysis of soil-structure interaction during earthquakes initiated with the finite element method in the 1960s. They have gone through various stages, but always in two distinct directions, that is, the substructure method and the direct method, depending on the modeling method for soil around the structures. For long time, modeling of dynamic soil-structure interaction was carried out in the frequency-domain, which restricted the analysis of the soil-structure system to be linear. Nonlinearity of the soil was taken into account only in an approximate manner through equivalent linear analysis procedure in which dynamic soil parameters were adjusted in accordance with the peak or the average strain during iterative solutions of the system frequency-domain. Substructure method is usually solved using frequency-domain therefore the structure had to be assumed to be linear.

Direct method is then developed to address this problem which went to time-domain using well-established procedure of structural dynamics. Initially, direct method can not model the energy radiation effect which well-understood using sub-structure method under frequency-domain. In response, there began in the direct method the development of transmitting boundaries, such as early viscous boundary proposed by Lysmer and then various kinds of consistent boundaries. Both kind of boundaries are presented in **Figure 2.19.** The general purpose of these transmitting boundaries are to avoid the reflection of waves emanating from the strucuture and the adjacent soil.

More recent research of dynamic soil-strucuture modeling tends to be concentrated in the time-domain, not only because the problem non-linearity can be better simulated in time-domain than in frequency-domain, but also that the typical stuctural analyst is not accustomed to working in the frequency-domain. The main difference between two models is that the transmitting boundaries of the direct method should be uncoupled both in time and space, which leads to approximate expressions for the boundaries. Whereas in the substructure method, the dynamic stiffness matrix can be obtain rigorously in the frequency-domain using convolution theorem of Fourier Transform.

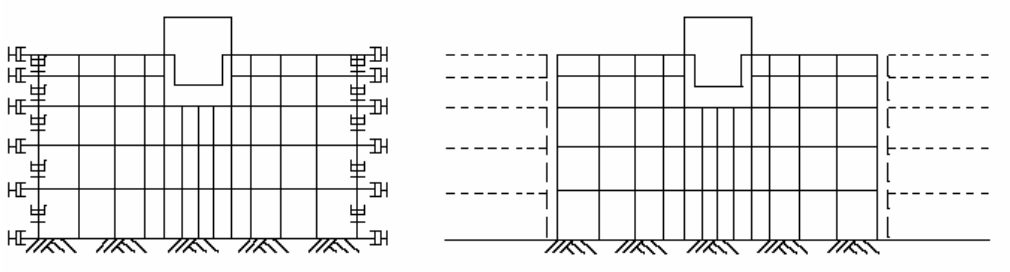

(a) (b)

Figure 2.19 Schematic representation of (a) Viscous Boundary and (b) Consistent Boundary

It should be pointed out that numerical modeling of dynamic soil-structure interaction is still in its course of development. There are still no standard numerical models available. The various current models are no longer restricted only in the time or frequency-domain alone. Techniques used to establish numerical models are not restricited to be finite element or boundary element method. On the contrary, all these are always incorporated with one and another, and some new analysis techniques have been introduced such as the infinite element method.

II.5.2 Direct Method

In the direct method, the structure and the soil adjacent to it. As illustrated in **Figure 2.20**, free-field input motion are specified along the base and sides of the model an the resulting rsponse of interacting system is computed from the equations of motion,

$$[M]\{\ddot{u}\} + [K^*]\{u\} = [M]\{\ddot{u}_{ff}(t)\} \qquad \textbf{(2.15)}$$

Where $\{\ddot{u}_{ff}(t)\}$ are the specified free-field accelerations at the boundary nodal point.

It can be noted that the use of the direct method requires a computer program that can be treat the behavior of both soil and structure with equal rigor.

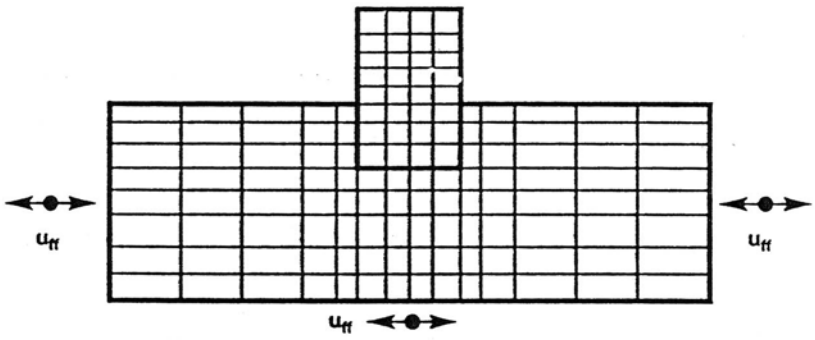

Figure 2.20 Direct method of soil-structure interaction analysis (after Kramer 1996)

II.5.3 Multistep or Sub-structure Method

Multistep or substructure methods use the principle of superposition to isolate the two primary causes of soil-strucuture interaction; the inability of the foundation to match the free-field deformation and the effect of the dynamic response of the structure – foundation system on the movement of supporting soil. The multistep method is the combination ofe kinematica and internial interaction.

- **Kinematic Interaction**

In the free field, an eartquake will cause soil displacements in both horizontal and vertical directions. If a foundation on surface of, or embedded in, a soil deposit is so stiff that it can not follow the free-filed deformation pattern, its motion will be influenced by kinematic interaction, even if it has no mass. The deformation due to kinematic interaction alone can be computed by assuming that the foundation has stiffness but no mass. The equation of motion for this case are

$$[M_{soil}]\{\ddot{u}_{KI}\} + [K^*]\{u_{KI}\} = -[M_{soil}]\{\ddot{u}_b(t)\} \qquad \textbf{(2.16)}$$

Where $[M_{soil}]$ is the mass matrix assuming that the structure and foundation are massless. The above equation describes the problem illustrated in **Figure 2.21**

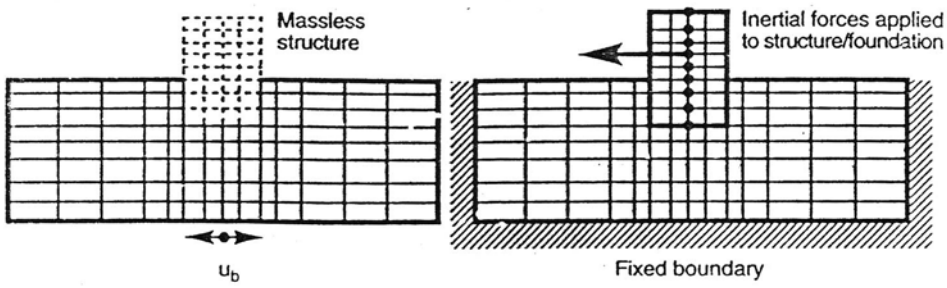

Figure 2.21 (a) Kinematic interaction analysis and (b) Inertial interaction analysis (after Kramer 1996)

- **Inertial Interaction**

The structure and the foundation have mass, and this mass cause them to respond dynamically. If the supporting soil is comliant, the forces transmitted to it by the foundation will produce foundation movement that would not occur in a fixed-base structure. The effects of soil compliance on the resulting response are due to inertial interaction. The deformation due to inertial interaction can be computed from the equations of motion

$$[M]\{\ddot{u}_{II}\} + [K^*]\{u_{II}\} = [M_{structure}]\{\ddot{u}_{KI}(t) + \ddot{u}_b(t)\} \qquad \textbf{(2.17)}$$

Where $[M_{structure}]$ is the mass matrix assuming that the soil is massless.

It is noted that the riht side of the above equation represents the inertial loading on the structure-foundation system.This inertial loading depends on the base motion and the foundation input motion, which reflects the effects of kinematic interaction. In the inertial interaction analysis, the inertial loading is applied only to structure while the base of the soil deposit is stationary.

- **Combination of Kinematic and Inertial Interaction**

The kinematic interaction analysis procedures the motion of the massless fundation-structure system (relative to the base) due to kinematic interaction.This motion is combined with the base motion to produces the total kinematic motion of the foundation-structure system. When the inertial loading that results from this kinematic motion is applied to the foundation-structure system resting on massless

soil, eguation (2.17) allows computation of the relative (to the total kinematic) motion. Adding eaquation (2.16) and (2.17) gives

$$[M_{soil}]\{\ddot{u}_{KI}\}+[M]\{\ddot{u}_{II}\}+[K^*](\{u_{KI}\}+\{\ddot{u}_{II}\})= \\ ([M_{soil}]+[M_{structure}])\{\ddot{u}_b\}-[M_{structure}]\{\ddot{u}_{KI}\} \quad \textbf{(2.18)}$$

Since $\{u_{KI}\}+\{u_{II}\} = \{u\}$ dan $[Ms_{oil}]+[M_{structure}] = [M]$, equation (2.18) is equivalent to the original equation of motion (2.15)

$$[M]\{\ddot{u}\}+[K^*]\{u\} = [M]\{\ddot{u}_b(t)\} \quad \textbf{(2.19)}$$

The above equation (2.19) proves that the solution to the entire soil-structure interaction problem is equal to the sum of the solutions of the kinematic and inertial interaction analyses.

II.6 An Introduction to Finite Element Procedures in Soil-Structure Interaction Analysis

If forces shake a structure at less than roughly one-third its lowest natural frequency of vibration, the problem can be treat as a static analysis. Therefore, the basic equation [K]{D} = {R} are accurate enough, even though loads {R} vary with time. More rapid shaking makes the inertia of the structure important, and the problem must be considered as dynamic analysis. Inertia is accounted by mass matrix, written as [m] for an element and as [M] for the whole observed structure and analogous to the damping matrix. In contrast to the static problem, [K] can be singular in a dynamic analysis, since the mass can holds structure together.

Problems in structural dynamics fit into two broad classes. The first is natural frequency of vibration analysis and corresponding modes shapes. The other is how the structure moves with time under a prescribed load, impulse or ground acceleration. The methods of structural dynamics are largely independent of finite element of finite element analysis because these methods presume the availability of stiffness, mass and damping matrices.

Mass and damping matrices, dynamic equations

D'Alembert's principle, while distasteful to some, easily leads to a defenition of the mass matrix and conveys its physical meaning. In the usual notation, an assumed element displacement field {f} = {u v w} and its first two time derivatives are

$$\{f\} = [N]\{d\}, \quad \{f\} = [N]\{\dot{d}\}, \qquad \{f\} = [N]\{\ddot{d}\}, \tag{2.20}$$

An acceleration field, $\{\ddot{f}\}$ produces d'Alembert body forces {F} in the opposite direction, so $\{F\} = -\rho \{\ddot{f}\}$, where ρ is mass density. Thus, nodal loads $\{r\}_\rho$ associated with {F} are re-build from the equation 2.1,

$$\{r\}_\rho = \int_V [N]^T \{F\} dV = -\int_V \rho [N]^T [N] dV \{\ddot{d}\} = -\{m\}\{\ddot{d}\} \tag{2.21}$$

And the element mass matrix [m] is defined as

$$[m] = \int_V \rho [N]^T [N] dV \tag{2.22}$$

Where [m] is known as the consistent mass matrix, [N] is shape function.

Following D'Alembert principle, dynamic loads is include inertia forces $\sum\{r\}_\rho$ and damping forces, $\sum[c]\{\dot{d}\}$ to form the governing equation of motion for the discretized system is as follows

$$\{R\} - [K]\{D\} - [C]\{D\} - [M]\{\ddot{D}\} = 0$$

$$\text{or} \qquad [K]\{D\} - [C]\{D\} - [M]\{\ddot{D}\} = \{R\} \tag{2.23}$$

Structural analysis is less interested in viscous damping, [c] than in dry friction and hysterisis loss. To investigate the energy-loss further, a common scheme is to combined a fraction α of the stiffness matrix with a fraction β of the mass matrix, written as

$$[C] = \alpha [K] + \beta [M] \tag{2.24}$$

Where, if $\alpha = 0$, the higher modes are lightly damped; if $\beta = 0$, the higher modes are heavily damped.

II.6.1 Numerical Accuracy and Stability

The accuracy of a numerical simulation of dynamic soil-structure interaction is controlled by two main parameters: a) the spacing of the nodes of the finite element (Δh) and b) the length of the time step (Δt).

- **Grid Spacing (Δh)**

In order to represent a traveling wave of a given frequency accurately about 10 nodes per wave length (λ) are required. Fewer that 10 nodes can lead to numerical damping as the discretization misses certain peaks of the wave. In order to determine appropriate maximum grid spacing the highest relevant frequency f_{max} that it present in the model needs to be found by performing a Fourier analysis of input motion. Typically, for sesimic analyses, f_{max} is about 10 Hz. By choosing the wavelength $\lambda_{min} = v/f_{max}$, where v is the wave velocity, to be represented by 10 nodes smallest wavelength that can be still be captured partially is $\lambda = 2\Delta h$, coressponding to a frequency of 5 Hz.

The maximum grid spacing should not exceed

$$\Delta h \leq \frac{\lambda}{10} = \frac{v}{10 f_{max}} \qquad \textbf{(2.25)}$$

Where v is lowest wave velocity (shear wave velocity in eneral)

- **Time step length (Δt)**

Time step Δt used for numerical solving nonlinear vibration or wave propagation problems has to be limited for two reasons. The stability requirement depends on the numerical procedure in use and is usually formulated in the form $\Delta t/T_n <$ value. T_n denotes the smallest fundamental period of the system. Similar to the spatial discretization, T_n needs to be represented by about 10 time steps. While the accuracy requirement provides a measureon which higher modes of vibration are

represented with sufficient accuracy, the stability criterion need to be satisfied for all modes. If the stability criterion is not satisfiedfor all modes of vibration, then the solution may diverge. In many cases it is necessary to provide an upper bound to the frequencies that are present in a system by including frequency dependent damping to the model.

Thesecond stabiity criterion results from the nature of the finite element method. As a wave front progresses in space it reaches one point after the other. If the time step in the finite element analysis is too large the wave front can reach two consecutive elements at the sam moment. This would violate a fundamental property of wave propagation and can lead to instability. The time step therefore needs to be limited to

$$\Delta h \quad \leq \frac{\Delta h}{v} \qquad \textbf{(2.26)}$$

Where v is highest wave velocity (shear wave velocity in eneral)

II.6.2 Plaxis Dynamic; Finite element code for soil and rock analyses

Basic equation dynamic behavior

For the static condition, the equation [K]{u} = {F} are accurate enough, even though loads vector {F} vary with time. Otherwise, the basic equation for the time-dependent movement of a volume under the influence a dynamic load (i.e. earthquake, wave, vibration) is

$$[M]\{\ddot{u}\} + [C]\{\dot{u}\} + [K]\{u\} = \{F\} \qquad \textbf{(2.27)}$$

Where [C] is the damping matrix that combined by mass matrix [M] and stiffness matrix [K], then displacement vector {u}, velocity vector $\{\dot{u}\}$, acceleration vector $\{\ddot{u}\}$ can vary in time. And {F} is a load vector.

The matrix C reflects the material damping which is caused by friction or by irreversible deformations (plasticity or viscosity). The greater the viscosity or the greater the occurrence of plasticity, the more vibration energy is dissipated, and

the less the material move after applying the particular load. To determine the damping matrix, [C], extra parameters are required, which are difficult to determine from tests, therefore is often written as a combination of the mass matrix and the stiffness matrix as the following;

$$[C] = \alpha_R [M] + \beta_R [K] \qquad \textbf{(2.28)}$$

Where α_R and β_R are the Rayleigh coefficients as the limit to determine the damping matrix.

When the share of [M] in [C] is greater, more of the low frequency vibrations are damped, and the share [K] in [C] is greater, more of the high frequency is damped.

Time Integration

In the numeric implementation of dynamics, the form of integration is the determining factor for the stability and accuracy of the calculation process. The Newmark scheme is a frequently used method of implicit time integration. With this method, the displacement and the velocity at the point in time t+Δt are written respectively as:

$$u^{t+\Delta t} = u^t + \dot{u}^t \Delta t + \left((1/2 - \alpha)\ddot{u}^t + \alpha \ddot{u}^{t+\Delta t} \right) \Delta t^2 \qquad \textbf{(2.29)}$$

$$\dot{u}^{t+\Delta t} = \dot{u}^t \left((1 - \beta)\ddot{u}^t + \beta \ddot{u}^{t+\Delta t} \right) \Delta t \qquad \textbf{(2.30)}$$

Where Δt is the time step, α and β are the coefficients to determine the accuracy of the numeric time integration. In order to obtain a stable solution, the following condition must apply:

$$\beta \geq 0{,}5 \qquad \alpha \geq 1/4(0.5 + \beta)^2 \qquad \textbf{(2.31)}$$

Implementation of the integration scheme in Plaxis

The equations (3.2) can also be written as,

$$\ddot{u}^{t+\Delta t} = c_0 \Delta u - c_2 \dot{u}^{t} - c_3 \ddot{u}^{t}$$

$$\dot{u}^{t+\Delta t} = \dot{u}^{t} + c_6 \ddot{u}^{t} + c_7 \ddot{u}^{t+\Delta t}$$

$$u^{t+\Delta t} = u^{t} + \Delta u \qquad \textbf{(2.32)}$$

or as

$$\ddot{u}^{t+\Delta t} = c_0 \Delta u - c_2 \dot{u}^{t} - c_3 \ddot{u}^{t}$$

$$\dot{u}^{t+\Delta t} = c_1 \Delta u - c_4 \dot{u}^{t} + c_5 \ddot{u}^{t}$$

$$u^{t+\Delta t} = u^{t} + \Delta u \qquad \textbf{(2.33)}$$

Where c_0, c_1, …, c_7 can be expressed in the time step and in the integration parameters α and β.

With implicit time integration, equation (3.1) must be compiled with the end of a time step ($t+\Delta t$):

$$[M]\{\ddot{u}^{t+\Delta t}\} + [C]\{\dot{u}^{t+\Delta t}\} + [K]\{u^{t+\Delta t}\} = \{F^{t+\Delta t}\} \qquad \textbf{(2.34)}$$

This equation, combined with the expressions (3.4) for the displacements, velocities, accelerations at the end of the time step, produce

$$(c_0[M] + c_1[C] + [K])\Delta\{u\} =$$

$$\{F\}_{ext}^{t+\Delta t} + [M]\left(c_2\{\dot{u}\}^{t} + c_3\{\ddot{u}\}^{t}\right) + [C]\left(c_4\{\dot{u}\}^{t} + c_5\{\ddot{u}\}^{t}\right) - \{F\}_{int}^{t} \qquad \textbf{(2.35)}$$

In this form, the equation system for a dynamic analysis reasonably matches that of a static analysis. The difference is that the 'stiffness matrix' contains extra terms for mass and damping and that right-hand term contains extra terms specifying the velocity and acceleration at the start of the time step (time Δt).

Wave Velocities

The compression wave velocity, Vp, depends on the one-dimensional stiffness and the mass of the medium:

$$V_p = \sqrt{\frac{(1-\upsilon)E}{\rho(1+\upsilon)(1-2\upsilon)}} \qquad \textbf{(2.36)}$$

for the shear wave velocity, Vs:

$$V_s = \sqrt{\frac{E}{2\rho(1+\upsilon)}} \qquad \textbf{(2.37)}$$

Where E = Young's Modulus, ν = Poisson's ratio

Critical Time Stepping

Despite the implicit integration, the time step used in the calculation is subject to limitations. If the time step is too large, the solution will display major deviations and the calculated response will be unreliable. The critical time step depends on the maximum frequency occurring in the model and the accuracy of finite element mesh. The general form of critical time step is written as follows:

$$\Delta t_{critical} = \frac{B}{\alpha\sqrt{\frac{E(1-\upsilon)}{\rho(1+\upsilon)(1-2\zeta)}}\sqrt{1+\frac{B^4}{4S^2}-\frac{B^2}{2S}\left[1+\frac{1-2\upsilon}{4}\frac{2S}{B^2}\right]}} \qquad \textbf{(2.38)}$$

Where, α factor depends on the element type (for a 15-node element, ($\alpha=1/19\sqrt{c_{15}}$, c_{15}=4,9479), ν is Poisson's ratio, B is average length of element, and S is surface area of the element. In a finite element model, the critical time step is equal to the minimum value of Δt according to over all elements.

Model Boundaries

For dynamic calculations, the boundaries should in principle be much further away than for static deformation calculations because vibrations generally disperse very quickly. To counteract reflections, special measures are needed at time boundaries, which is known by absorbent boundaries. This absorbent boundary is used for modeling the limitation of finite element geometry model. The use of absorbent boundaries in Plaxis, is based on the method described by Lysmer and Kuhlmeyer.

The normal stress and shear stress components absorbed by damper in X-direction are:

$$\sigma_n = -C_1 \rho V_p \dot{u}_x \qquad \textbf{(2.39)}$$

$$\tau = -C_2 \rho V_s \dot{u}_y \qquad \textbf{(2.40)}$$

Where, ρ is density of the materials, and C_1 and C_2 relaxation coefficient that introduces the effect of absorption.